

2D and 3D discrete numerical modelling of soil arching^{*}

Ning BAO¹, Jing WEI^{†‡1}, Jian-feng CHEN², Ping WEI³

¹School of Civil Engineering, Beijing Jiaotong University, Beijing 100044, China

²School of Civil Engineering, Tongji University, Shanghai 200092, China

³School of Engineering and Surveying, Beijing Polytechnic College, Beijing 100042, China

[†]E-mail: jingwei@bjtu.edu.cn

Received Dec. 29, 2019; Revision accepted Mar. 18, 2020; Crosschecked Apr. 14, 2020

Abstract: In this study, 2D and 3D soil arching phenomena associated with piled embankments were evaluated by performing a series of discrete numerical analyses using the particle flow code (PFC3D) software. After validating the micro-parameters with experimental results, we compared the stress-displacement distribution, force chain evolution, maximum vertical displacement of particles, and deformation characteristics induced by 2D and 3D arching effects. Additional analyses were carried out to understand the influence of the fill height, pile clear spacing, friction coefficient, and porosity on soil arching with respect to the stress concentration ratio (SCR) and settlement along the elevation at various sections. The numerical results indicated that a plane soil arch in a 2D embankment overestimates the degree of load transfer and underestimates the settlement at the crest and within the embankment along the elevation in a 3D embankment. A lower equal settlement plane can be found in a 2D embankment. Furthermore, an increase of fill height and friction angle, and a decrease of pile clear spacing and porosity can help to improve the degree of reduction in load transfer and settlement in both 2D and 3D embankments. However, for partially mobilized soil arching in the 3D condition, the increase of fill height reduces the settlement of soils mainly in the portion above the square subsoil area, but has less influence over the portion above the rectangular subsoil area.

Key words: Piled embankment; Soil arching; Discrete element method (DEM); Load transfer; Settlement
<https://doi.org/10.1631/jzus.A1900672>

CLC number: U416.12

1 Introduction

Many improvement techniques like pile foundations, earth platforms, stone columns, and reinforcement may need to be adopted when geotechnical structures are constructed on soft ground (Han and Gabr, 2002; Jenck et al., 2007; Bhandari and Han, 2010; van Eekelen et al., 2020). A closely spaced piled embankment is one of the traditional methods to control large embankment settlement at reduced cost in a short period of time. In a pile-supported embankment, relatively large loads are transferred to the pile caps due to

the occurrence of soil arching. The importance of soil arching in the load transfer mechanism of geotechnical structures has been highlighted by Terzaghi (1943). Several researchers have tried to demonstrate the soil arching mechanism using trapdoor model tests (Chen et al., 2008; Costa et al., 2009; Zhu et al., 2012; Iglesia et al., 2014; Rui et al., 2016a, 2016b, 2019; Bhandari and Han, 2018), computed tomography (CT) scanning (Chevalier and Otani, 2011; Eskişar et al., 2012), and full-scale model tests (Briçon and Simon, 2012; King et al., 2017; van Eekelen et al., 2020). Among these tests, trapdoor model tests are considered to be a simple way to comprehend the soil arching phenomenon. The most commonly adopted trapdoor configurations are plane strain single- or multi-trapdoor tests and 3D trapdoor tests (Rui et al., 2019). The plane-strain trapdoor model corresponds to a plane soil arch and the 3D trapdoor model to a spatial soil arch.

[‡] Corresponding author

^{*} Project supported by the National Natural Science Foundation of China (No. 41772289)

 ORCID: Ning BAO, <https://orcid.org/0000-0002-2512-761X>

© Zhejiang University and Springer-Verlag GmbH Germany, part of Springer Nature 2020

The numerical and laboratory results of plane soil arches indicate that the settlement (Δs) of the trapdoor is a key factor governing the evolution of soil arching (Ladanyi and Hoyaux, 1969; Dewoolkar et al., 2007; Chen et al., 2008; Lai et al., 2016; Rui et al., 2016a, 2016b, 2019; Han et al., 2017; Bhandari and Han, 2018). Iglesia et al. (2014) performed a centrifuge model trapdoor test and observed three arch patterns, namely curved arch, triangular arch, and rectangular arch, with trapdoor sinking. To link the soil arching with support from the subsoil, Iglesia et al. (2011, 2014) proposed a ground reaction curve (GRC) to describe the evolution of arching by classifying it into four stages: the initial arching stage, the maximum arching stage, the loading recovery stage, and the ultimate stage. In the GRC, the first two phases can be considered as the arching enhanced stage, and the load recovery condition corresponds to the arching weakened stage. King et al. (2017) monitored the regional rail link in Melbourne, Australia to investigate the variation in the stress response of the load transfer platform in all four stages. They reported that the stress recovery stage was the most important phase in the column-supported embankment design, because it predicted the breakdown of the arching stresses. Besides the settlement of the trapdoor, geometric and geotechnical parameters, such as the embankment height h , pile spacing, cap size a , internal friction angle ϕ , and porosity, also dictate the formation and features of soil arching. Jenck et al. (2007, 2009a) studied the effect of platform properties on the degree of load transfer and surface settlement. Rui et al. (2019) classified the arching evolution pattern into triangular expanding patterns, tower-shaped patterns, and equal settlement patterns in unreinforced embankments with different fill heights and cap widths using a particle image velocimetry (PIV) technique. Not only those internal factors, but also a few other external factors have a significant influence. For example, Song et al. (2018) found that at a certain water table depth, a further increase in the water table would enlarge the arch height and weaken the soil arching through recovering more load onto the trapdoor. Xu et al. (2019) indicated that static and cyclic loading would cause degradation of soil arching.

For a spatial soil arch, wheel load and embankment load are transferred onto the parallel and

diagonal piles in the 3D embankment, but only onto the parallel piles in the 2D embankment. In other words, the mechanical and deformation mechanism in 3D embankments is more complex. Over the past three decades, empirical models, such as Marston (1930)'s model adopted by BS8006-1 (BSI, 2010), frictional models, such as Russell et al. (2003)'s model extended from Terzaghi (1943)'s plane model, limit state equilibrium models, such as Hewlett and Randolph (1988)'s model, Kempfert et al. (2004)'s model, and van Eekelen et al. (2012a, 2012b)'s model, have been proposed to describe the shape of the arch based on experimental observations and theoretical analysis. The results from such analyses were inconsistent, possibly due to assumptions made in the formulation to depict the load transfer in 3D conditions (Rowe and Liu, 2015). The mechanical response of the embankment was investigated by several researchers through 3D numerical analysis using finite element method (FEM), finite difference method (FDM), and discrete element method (DEM) approaches (Jenck et al., 2009b; Le Hello and Villard, 2009; Zhuang and Wang, 2015; Das and Deb, 2018; Badakhshan et al., 2020). Tran et al. (2019) compared the performance of piled embankments through FDM and DEM and concluded that DEM gave a better representation of discontinuities and large displacements. From a detailed literature review we noted that very little research work has been carried out using DEM to explore spatial soil arching.

Although the load transfer and deformation mechanisms within piled embankments have been studied considering 2D and 3D modelling aspects, little research has been carried out to understand the similarities and differences between plane and spatial arches, which hinders the process of integrating the research results. In addition, earlier studies focused mainly on the deformation either at the crest or at the base of the embankment, but the variation of the settlement along the depth within the embankment fill has not been investigated. In the present study, a series of 2D and 3D DEM trapdoor models were developed using the particle flow code (PFC3D) software to understand the response of plane and spatial arches. Micro-parameters determined from triaxial tests were used to validate the numerical results. The effects of geometric and geotechnical parameters including fill height, pile clear spacing,

friction coefficient, and porosity of fill were investigated in terms of the stress concentration ratio (SCR) and soil settlement along the depth in various sections.

2 Numerical modelling

2.1 Modelling details for simulation procedure

The 3D trapdoor model tests carried out by Cao and Hu (2014) were chosen for this study to simulate the trapdoor response in 2D and 3D conditions using discrete element modelling. In this section, we briefly summarize the apparatus used, the testing procedure, and details of the relevant properties. Fig. 1 shows a schematic view of the trapdoor model. Considering the symmetry of the embankment and neglecting the influence of the sloping portion of the embankment, a portion of the embankment above the four piles was designed to act as a unit cell. The trapdoor model comprised bricked bases as rigid square piles, toughened glass side walls, and a cross-shaped water bag as a displacement controller. The gradual release of water from the water bag was used to simulate the trapdoor condition. The embankment was made up of medium coarse sand ($D_{50}=0.4$ mm) having a unit weight of 17.63 kN/m³ and peak friction angle of 32° . Earth pressure cells were placed on top of the pile caps and water bag, to continuously record changes in the stress condition. This test setup can be considered an improved version of the 2D trapdoor model designed by Chen et al. (2008), which was used to quantitatively measure the plane soil arching effect.

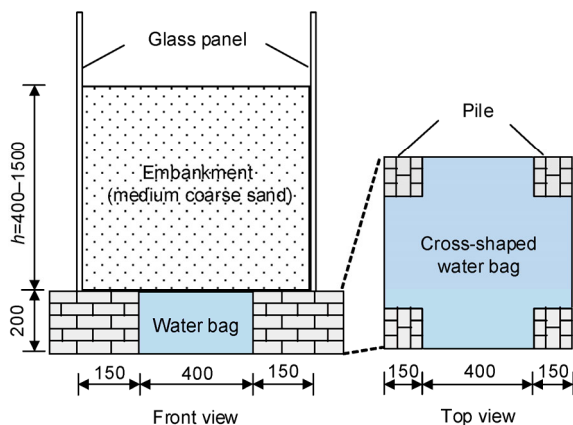


Fig. 1 Schematic representation of the 3D trapdoor experimental model (unit: mm)

Fig. 2 shows the 2D and 3D DEM trapdoor model simulated using the PFC3D software developed by Itasca, USA. The 2D DEM trapdoor model with the embankment founded on two piles is considered a subset of a 3D embankment, considering the dimensions of the pile caps and pile clear spacing. The sand particles were idealized as spherical particles (i.e., balls) with a linear contact model. The improved multi-layer compaction method (IMCM) proposed by Lai et al. (2014) was used to uniformly generate balls at a specific porosity and with a particle size ranging from 16 to 22 mm. With the increase in the height of the embankment from 0.6 to 1.4 m, a significant increase in the number of balls from 48 115 to 112 796, with an average porosity of 0.4 was observed after reaching the gravity balance stage. Walls with smooth surfaces were used to model the rigid piles, side walls, and trapdoor. As the lateral displacement of the side walls was restricted, only vertical displacement was considered. Measuring spheres of 50 mm in diameter were distributed uniformly to monitor the change in the state of stress.

To understand the spatial characteristics of the soil arch, the 3D embankment was zoned into three parts (Fig. 2): a portion above the square subsoil

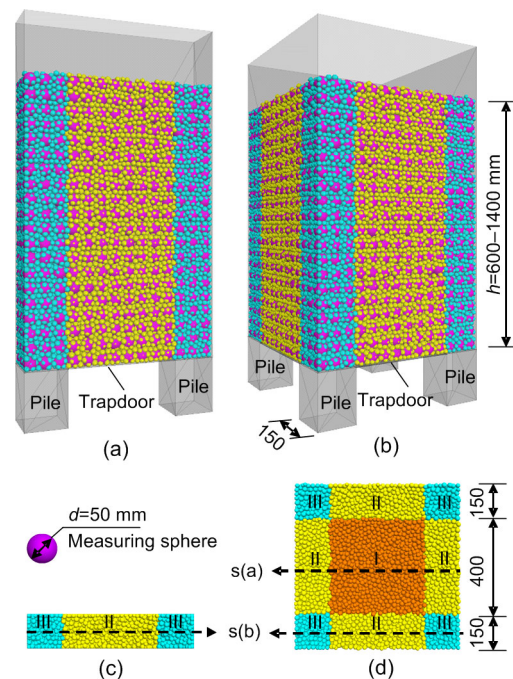


Fig. 2 2D and 3D DEM trapdoor models (unit: mm)
(a) Oblique view, 2D; (b) Oblique view, 3D; (c) Top view, 2D;
(d) Top view, 3D

between the four piles (Part I), a portion above the subsoil between the parallel piles (Part II), and a portion above the four pile caps (Part III). To monitor the settlement of particles along the depth, two sections (namely, s(a) and s(b)) in the middle of Parts I and II were selected.

2.2 Determination of micro-parameter

In DEM, micro-parameters of model components (e.g. balls, walls, and contact models) govern the macro-mechanical response. Numerical geotechnical tests are often used to calibrate the micro-parameters by trial and error. In this study, a series of triaxial tests were simulated to obtain the stress-strain characteristics of particle assembly. About 4049 balls with a diameter ranging from 16 to 22 mm were filled into the triaxial specimen (0.50 m high and 0.25 m wide) made of walls using the IMCM, with a porosity of 0.4 (like the embankment fill). A linear contact model was assigned to ball-ball and ball-facet contacts. Typical confining pressures (e.g. 20, 30, and 50 kPa) were selected to consolidate the sample (based on the servo mechanism). After the consolidation stage, the top wall was allowed to move downward at a constant velocity (1 mm/s) to simulate shearing of the sample. The velocity was selected such that the dynamic effect induced by fast loading was minimized (Andrade et al., 2012). Fig. 3 shows the simulated triaxial test results. The stress-strain curve shows that hardening behavior was observed at a relatively low axial strain level (<1%), followed by softening behavior. The numerically obtained peak friction angle (31.4°) was in good agreement with the experimentally observed value. The micro-parameters adopted in the DEM simulation are listed in Table 1.

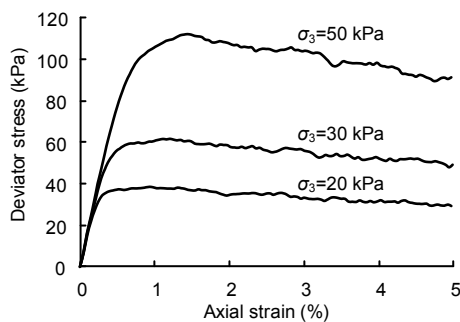


Fig. 3 Stress-strain relationship from PFC3D triaxial tests
 σ_3 is the confining pressure

The velocity of trapdoor movement may have some influence on the mechanical response of the embankment fill. If the trapdoor moves at a fast velocity, then the particles at the base may lose contact temporarily because of the restriction of calculation efficiency, and then may fall quickly leading to higher stress fluctuations. In contrast, if the trapdoor moves slowly, then the fluctuations in stress can be reduced significantly, and the simulation time might increase (especially for the 3D DEM simulation). To evaluate the influence of the velocity of trapdoor movement, four different downward velocities ranging from 5 to 20 mm/s were chosen in this study. Fig. 4 shows the variation of average earth pressure on the pile caps, σ_p , with an embankment height of 0.6 m as the trapdoor moves downward. Note that as the settlement rate increases, fluctuations in earth pressure

Table 1 Micro-parameters used in the DEM model

Parameter	Value	
	Ball	Wall
Porosity	0.4	–
Particle density (kg/m ³)	1650	–
Local damping ratio	0.7	–
Friction coefficient	1.0	0.0
Normal contact stiffness, k_n (N/m)	1.0×10^6	1.0×10^{10}
Shear contact stiffness, k_s (N/m)	0.5×10^6	1.0×10^{10}

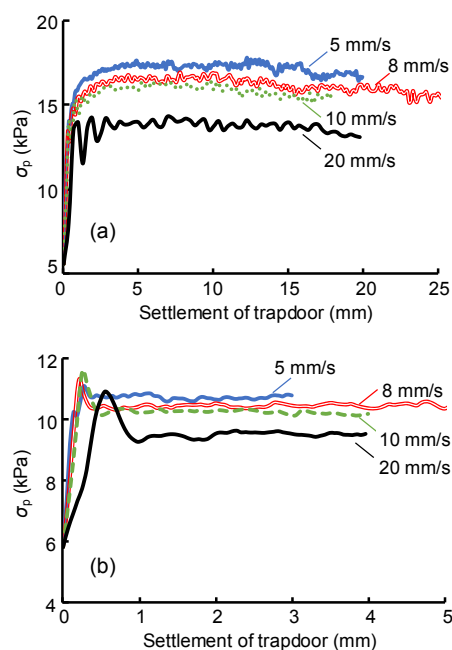


Fig. 4 Variation of average earth pressure with trapdoor settlement considering different settlement velocities
 (a) 3D model; (b) 2D model

become more prominent. The velocity threshold lies between 10 and 20 mm/s. The magnitude of earth pressure predicted by considering lower downward velocity is higher than that predicted by considering faster velocity. The pressure difference is about 5%–10% when velocity is slower than 10 mm/s. Taking the stress fluctuation effect and computation cost into account, a velocity of 8 mm/s was chosen for the 3D trapdoor numerical model. The 2D numerical model, which is filled with about 1/5 of the particles of the 3D model, has a larger computation timestep, and thus runs faster than the 3D model. Therefore, a smaller rate of 5 mm/s for the 2D condition was selected to acquire a smaller stress fluctuation effect (Fig. 4b).

Fig. 5 shows a comparison of the results obtained from the numerical and experimental studies. The results from DEM are in agreement with the experimental results. The earth pressure acting on piles increases initially and then decreases slowly with the increase in the settlement of the trapdoor. The average earth pressure on the subsoil σ_s decreases with the increase of trapdoor settlement. For an embankment height of 1.4 m, the degree of soil arching increases (settlement of trapdoor $\Delta s < 8$ mm) and then weakens ($\Delta s > 8$ mm) during this process.

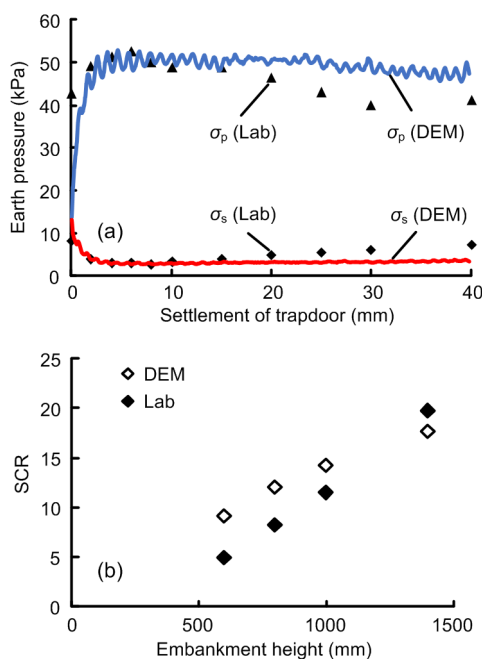


Fig. 5 Comparison of numerical (DEM) and experimental (lab) results: (a) earth pressure; (b) SCR

The SCR is defined as the ratio between the earth pressure acting on pile caps σ_p and the pressure acting on the subsoil σ_s (Han and Gabr, 2002; Chen et al., 2008; Das and Deb, 2018). The SCR is a representative parameter used to describe soil arching and the degree of load transfer; the higher the value, the larger the degree of load transfer. The maximum values of the SCR at different embankment heights are presented in Fig. 5b. As the height of the embankment increases, the SCR increases. The difference in the SCRs obtained from DEM and from experiment diminishes with the increase in the height of the embankment. At the initial stage ($\Delta s = 0$ mm), stresses on the pile surface and subsoil are not identical in the case of the model test, possibly due to the compressibility and free mobility characteristics of the water bag. This leads to the formation of soil arching at the initial stage of embankment load, unlike with the rigid trapdoor adopted in DEM. At the arching weakened stage ($\Delta s > 10$ mm), the decrease of earth pressure acting on the piles and the increase of pressure on the subsoil obtained from the DEM model are smaller than those obtained from the laboratory results. This may be because of the larger particles adopted in DEM than in the test sand. Larger particles can form a stable structure easily due to surface friction, and can offer more resistance to soil disturbance than smaller particles. As discussed above, the DEM model can represent the mechanical response of piled embankments influenced by arching, and the validation of micro-parameters allows for further analysis and parametric study.

3 Analysis and interpretation

Based on the critical embankment height h_{cr} , the soil arching in the piled embankments can be classified as fully mobilized soil arching (embankment height $h \geq h_{cr}$) or partially mobilized soil arching ($h < h_{cr}$). However, determination of the critical embankment height depends on the choice of arching models. The frictional model proposed by Terzaghi (1943) suggested h_{cr} equal to $1.5B-2.5B$ (B is the pile clear spacing). The limit state equilibrium model proposed by Hewlett and Randolph (1988) recommended $h_{cr} = 0.5(B+a)$ (for the 2D case) or $0.7(B+a)$ (for the 3D case with square pile caps), and the empirical model BS8006-1 (BSI, 2010) considered

$h_{cr}=1.4B$. To investigate the stress response and occurrence of deformation during the development of a fully mobilized soil arching, a 3D embankment of height 1.0 m ($2.5B$) was selected and compared with the response of a 2D embankment.

3.1 Stress-displacement response

Fig. 6 shows the variation of the soil arching ratio ρ (defined as the ratio of the average vertical stress on the subsoil σ_s to the initial stress acting on the subsoil σ_0) with normalized displacement (displacement Δs with respect to pile clear spacing B). The results indicate that 2D and 3D stress-displacement curves show typical characteristics of a GRC curve: there is a sharp decrease (initial stage) to a minimum value (maximum arching stage), followed by a gradual increase (loading recovery stage). However, in the arching enhanced stage, the subsoil stress of the 2D trapdoor model decreases at a higher rate and reaches a lower minimum value ($\rho_{2D}=0.13$) at $\Delta s/B=0.65\%$ than $\rho_{3D}=0.31$ at $\Delta s/B=2.11\%$ of the 3D model. This comparison indicates that a plane soil arch can transfer more load onto the piles with less settlement, while a spatial soil arch demands more settlement to fully achieve the degree of arching.

In the process of embankment deformation, a change in the porosity of fills is inevitable (Costa et al., 2009; Han et al., 2012; Badakhshan et al., 2020). Fig. 7 depicts the change in the average porosity at various stages of soil arching. Porosity remains constant at the arching enhanced stage in both 2D and 3D models. Given the spherical surface of balls, interlocking between particles can be neglected; hence, embankment fill transfers its weight above the trapdoor to the pile caps through the surface friction of particles. In other words, the arching enhanced stage corresponds to the increase of the static friction force. In the loading recovery stage, the subsoil stress increases gradually, and the arching effect attenuates to some extent. At this stage, the porosity of the embankment fill increases gradually, indicating a trend of dilation, leading to a reduction in the shear strength of the soil. With trapdoor sinking, the relative movement between particles increases, and the surface static friction force is transformed into a sliding friction force, thereby weakening the ability of load transfer through the shear force.

For soil at the ultimate stage, Terzaghi (1943) considered the vertical slip surface of a 2D trapdoor

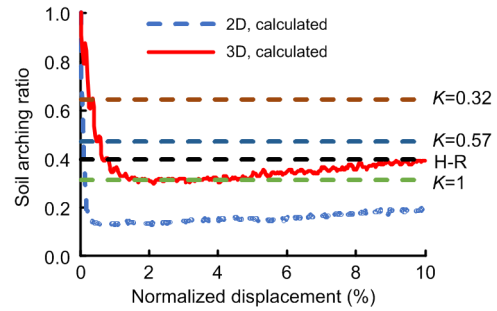


Fig. 6 Evolution of the soil arching ratio with trapdoor settlement (K is the lateral earth pressure coefficient; H-R indicates Hewlett and Randolph (1988)'s model)

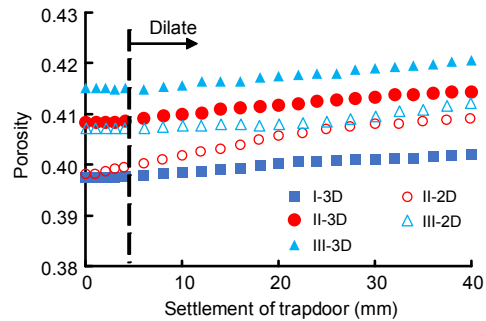


Fig. 7 Porosity changes with settlement (I-3D means Part I in the 3D model)

model and derived an expression for determining the vertical stress acting on the trapdoor (Eq. (1), with no consideration of cohesion). Terzaghi (1943) recommended the value of $K=1.0$ based on laboratory test results, but Marston (1930) suggested a value of K equivalent to active earth pressure ($K=K_a=\tan^2(45-\varphi/2)$) and Tien (1996) obtained the value of K ($K=\cos^2\varphi/(1+\sin^2\varphi)$) based on the vertical stress at critical state. In the case of 3D piled embankments, Hewlett and Randolph (1988)'s model assumed that the arch was a hemisphere and derived the equilibrium equation of the element at the crown of the soil arch and at the pile top, as given in Eqs. (2) and (3). The ultimate value was taken as the larger of the two ($\rho_{pile-top}=0.398$, $\rho_{arch-top}=0.255$). It can be observed from Fig. 6 that ρ increases as K decreases. Terzaghi (1943)'s model has underestimated the degree of plane soil arch, but the H-R model has accurately predicted the ultimate stage of the evolution of the spatial arch.

$$\rho = \frac{B}{2hK \tan \varphi} \left(1 - e^{-\frac{2hK \tan \varphi}{B}} \right), \quad (1)$$

$$\rho_{\text{pile-top}} = \frac{1}{\left(\frac{2K_p}{1+K_p}\right) \left[\left(1-\frac{a}{s}\right)^{1-K_p} - \left(1-\frac{a}{s}\right) \left(1+\frac{a}{s}K_p\right) \right] + \left(1-\frac{a^2}{s^2}\right)}, \quad (2)$$

$$\rho_{\text{arch-top}} = \left(1-\frac{a}{s}\right)^{2(K_p-1)} \left[1 - \frac{\sqrt{2}s(K_p-1)}{h(2K_p-3)} \right] + \frac{\sqrt{2}(s-a)(K_p-1)}{h(2K_p-3)}, \quad (3)$$

where a is the cap size of the pile, s is the pile spacing, and K_p is the passive earth pressure coefficient ($K_p = \tan^2(45 - \varphi/2)$).

Soil arching is a stress redistribution effect which changes not only the load distribution on the pile top and subsoil, but also the stress transmission path within the embankment. Han et al. (2012) pointed out that the load transfer in the embankment is due to the reorientation of major principal stress. Fig. 8 shows the contour of major principal stress σ_1 at section s(b) (refer to Fig. 2 for location) in both the 2D and 3D models at $\Delta s = 40$ mm calculated from measuring spheres. After the occurrence of the soil arching effect, the transmission path of major principal stress deviates from a vertical distribution; σ_1 increases above the pile caps, but decreases between the pile caps, and remains unaffected at the top level of the embankment. The major principal stress at the pile top in the 2D model (25.2 kPa) is less than that in the 3D model (34.2 kPa).

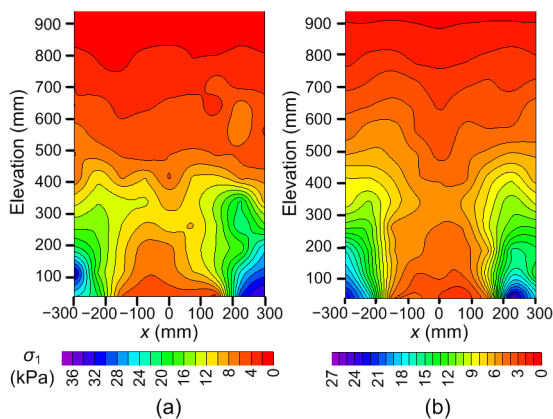


Fig. 8 Contour of σ_1 of section s(b)
(a) 3D model; (b) 2D model

3.2 Force chains

In the DEM model, contact force is transmitted through contact between two balls and presented by the force chain showing its direction and relative magnitude. A strong force chain corresponds to a large contact force. Lai et al. (2014) found that strong contacts (contact force F_c above average contact force \bar{F}_c) formed the loading transmission path, and weak contacts served mainly as a support system. The strong contacts ratio is defined as the ratio of the number of strong contacts at a specific settlement to the number at the initial stage. Figs. 9 and 10 show the strong contacts ratio and the distribution of the developed strong force chain with the increase in the trapdoor settlement for the 2D and 3D models. The model with a strong contacts ratio for the whole embankment is termed the entire model-2D (or 3D).

At the initial stage, the strong force chains are distributed vertically, and the strong contacts ratio of different parts is about 0.4 in the 3D numerical model. As the settlement of the trapdoor increases, arching steps into the enhanced stage and the strong contacts ratios in Parts I, II, and III reach 0.24, 0.33, and 0.43 at $\Delta s = 1$ mm, 6 mm, and 12 mm, respectively. With the fully mobilized soil arching effect achieved, the strong force chain concentrates on the

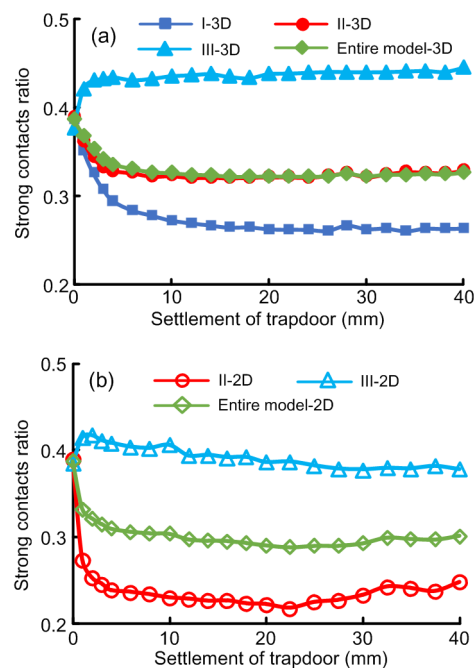


Fig. 9 Evolution of the strong contacts ratio
(a) 3D model; (b) 2D model

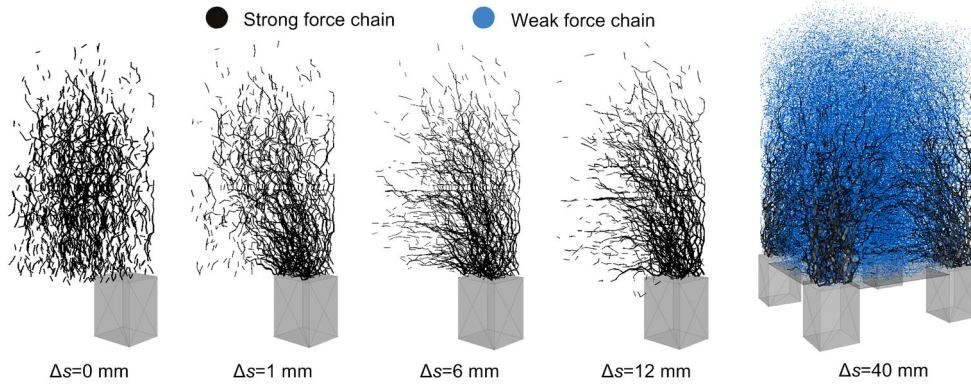


Fig. 10 Force chains developing with settlement of the trapdoor
The first four models each represent one quarter of the 3D model

pile caps and makes an extension between Parts I and II to form a spatial arch, and the soil load above the subsoil is transferred to the top of the pile through shear stresses. In the loading recovery stage, embankment fill shows a trend of dilation (Fig. 7) and a portion of the load transfers onto the subsoil, but the strong contacts ratio remains constant and the shape of the force chain is basically stable until $\Delta s=40$ mm, which implies that the loading recovery has less influence on the soil arch.

The difference in the strong contacts ratio for 2D and 3D numerical models is manifest mainly in two aspects. (1) In the 2D model, the strong contacts ratio in Part III decreases at the stress recovery stage, and then is maintained the same as the initial value (0.4), while in the 3D model the ratio increases and keeps stable. This may be because soils above the pile caps have a relatively small interaction area with soils only in Part II in the 2D model, in contrast to larger contact areas with Parts I and II in the 3D model. Hence, in the 2D model there is less restriction to resist dilation on soils above the pile caps during the shearing process. (2) The strong contacts ratio in Part II in the 2D model is smaller than that in the 3D model. This corresponds to a greater degree of load transfer achieved in the 2D model (Fig. 6). As the larger proportion of the embankment load is transmitted to the pile caps, relatively small strong contacts are formed at Part II.

Fig. 11 shows a further classification based on the magnitude of the contact force at $\Delta s=40$ mm. The probability is a measure of the number of contacts whose contact force lies between $F_{c(i)}$ and $F_{c(i+1)}$ expressed as a percentage of the total number of

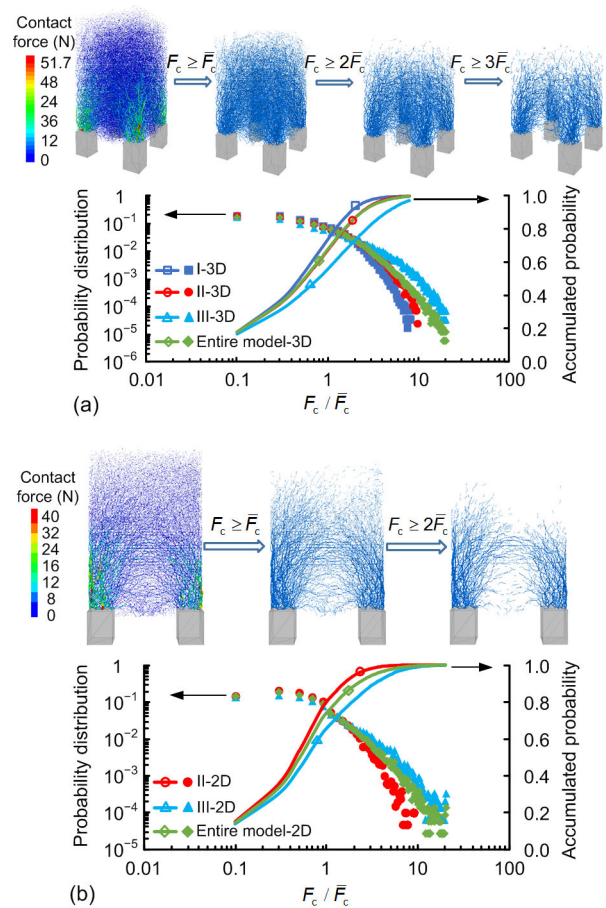


Fig. 11 Contact force probability distributions
(a) 3D model; (b) 2D model

contacts, where $F_{c(i)}=(i-1)\Delta F_c$ ($i \geq 1$). The contact force increment ΔF_c equals $0.1 \bar{F}_c$ in this study. The 2D and 3D models display a similar distribution feature: weak contacts exhibit regional independence and disperse mainly above the strong force arch. With

an increase in contact force, the proportion of strong contacts varies between Parts I, II, and III. The difference in the proportion increases with the increase in the contact force F_c , making the strong contacts ratio in Part III larger than that in Part II, and lowest in Part I. The arch structure made of the strong force chain presents a multi-arch phenomenon between Parts II and III, which is similar to the arch model proposed by Kempfert et al. (2004).

3.3 Maximum vertical displacement

As the trapdoor moves downward, subsidence of soil occurs at the midspan between the pile caps, and the displacement trajectory of particles declines along the elevation. The average settlement of particles at different sections in the range of $x=-50-50$ mm above the trapdoor is taken as the maximum vertical displacement so as to avoid local movement fluctuation (Fig. 12). A similar trend occurs in both the 2D and 3D models: the vertical displacement of particles increases gradually with trapdoor sinking and decreases as the measure height increases. The embankment deformation at sections s(a) and s(b) in the 3D model is almost the same when the trapdoor is lowered until it reaches 12 mm; with further lowering of the trapdoor, the vertical displacement at s(a)-3D (means s(a) in the 3D model) at the same elevation is larger than that at s(b)-3D due to the lower resistance of shear force. Moreover, the vertical displacement of s(b)-3D is larger than that of s(b)-2D at the same elevation, and the difference in the settlement increases gradually as the trapdoor moves down. At the maximum settlement of the trapdoor, the displacement of particles at the crest is 21% of the maximum Δs for the 2D embankment, which is nearly the same as the results of Bhandari and Han (2018), but 60% for the 3D embankment. This comparison indicates that the 2D embankment underestimates the settlement in the 3D condition.

There are equal settlement planes (ESPs) in both the 2D and 3D models when the differential displacement between adjacent measure heights in the embankment is close to zero (Fig. 12). The height of the ESP in the 3D model is between 400 and 600 mm, which is slightly larger than that in the 2D model (about 400 mm). Also, the ESPs in both the 2D and 3D models remain unchanged as the trapdoor comes down, which means that the soil arch structure remains stable after its formation.

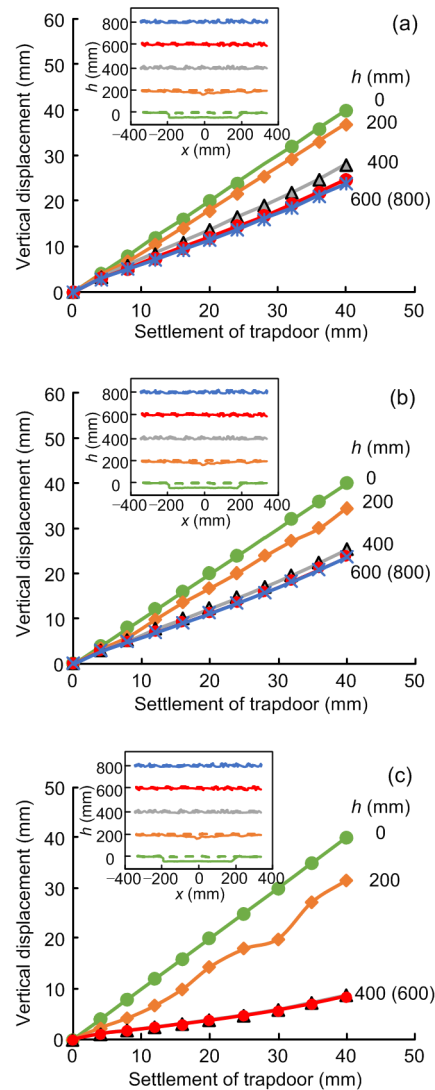


Fig. 12 Maximum vertical displacement plotted against settlement of the trapdoor

(a) Section s(a)-3D; (b) Section s(b)-3D; (c) Section s(b)-2D

3.4 Deformation characteristics

Fig. 13 shows a detailed comparison of soil settlement under the ESP ($h < 500$ mm) between the 2D and 3D models as Δs is lowered by 40 mm. The vertical displacement contour, settlement profiles, and vertical displacement grouping are shown in Figs. 14a–14c, respectively.

When the measure height h is lower than 0.1 m, the settlement at s(b)-3D is almost the same as that in the 2D model. As the measure height reaches 0.1 m, the average soil displacement is about 6.5 mm above the pile top and 40.0 mm above the trapdoor, and the

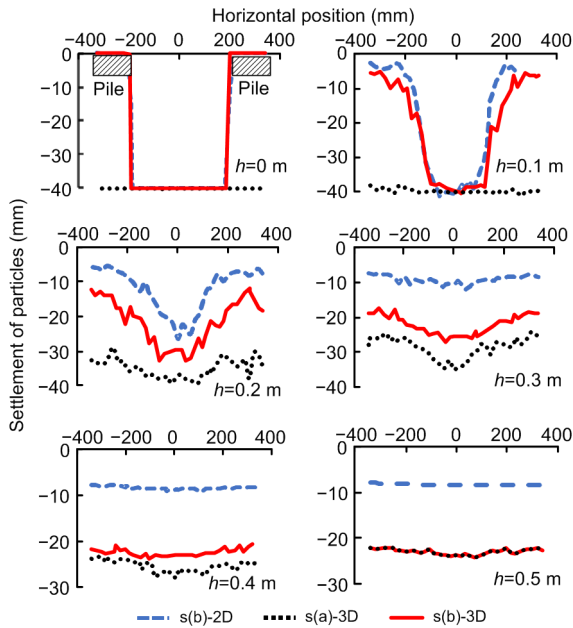


Fig. 13 Vertical displacement profiles at different sections along the elevation

differential settlement is 33.5 mm. A slip surface divides the larger settlement zone from the smaller settlement zone with an inclination angle of about $45^\circ + \varphi/2 = 61^\circ$ (Fig. 14a). As the measure height increases, a difference of settlement at section s(b) in the 2D and 3D models begins to appear, with the 3D model showing a larger settlement than the 2D model. A possible reason is that, in the 3D model, particles at Part I sink deeper than the surrounding fill forming the basin-like shape shown in Fig. 14b, due to a weaker influence of shear stresses. This results in a tendency to attract more particles in Parts II and III to move into the Part I area to balance the differential settlement.

Therefore, particles above two parallel piles in the 3D model can move vertically and horizontally, in contrast with particles in the 2D model moving only vertically, thus causing a larger loss of particles in Part II in the 3D model. Rothenburg and Bathurst (1993) also found a higher dilation rate of the 2D

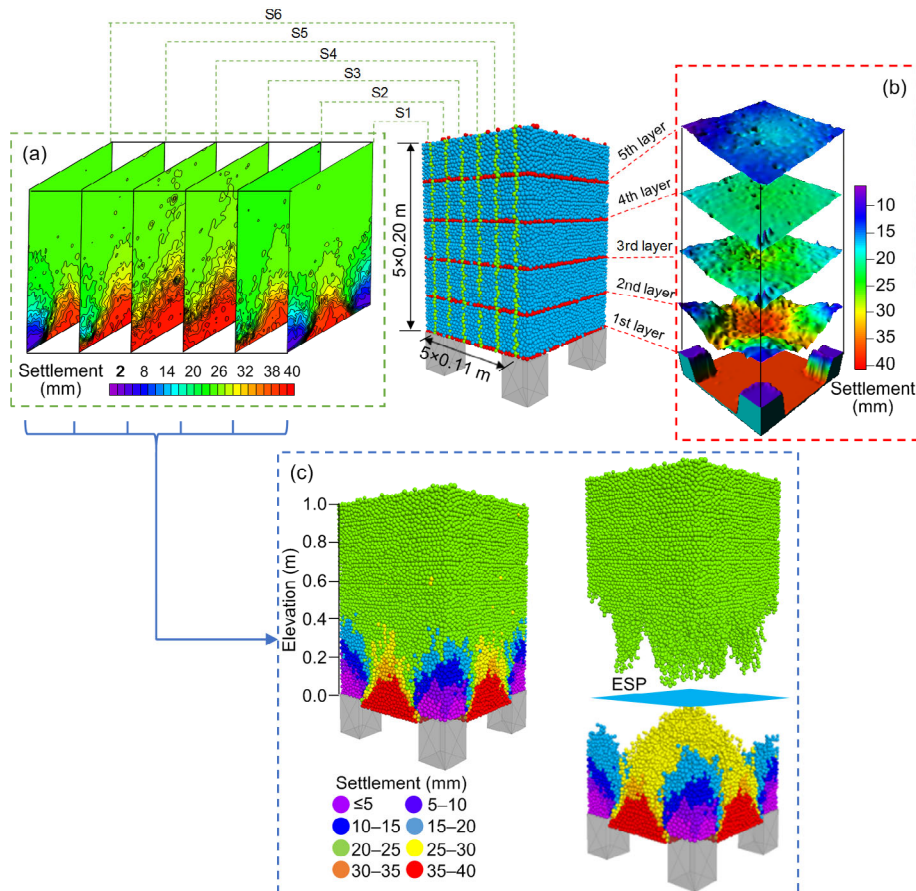


Fig. 14 Characteristics of deformation of the 3D piled embankment

(a) Vertical displacement contour; (b) Settlement profiles; (c) Vertical displacement grouping. $S(j)$ ($j=1, 2, \dots, 6$) indicates the j th vertical profile, and the distance between adjacent vertical profiles is 0.11 m

granular assembly than that of the 3D assembly, since the planar assembly could dilate only in one direction. As elevation is as high as 0.3 m ($<1.0B$), the 2D model reaches the ESP with a differential settlement of less than 2.6 mm. Below the ESP, the spatial soil arch acts like a dome (Fig. 14c). The height of the displacement arch above two parallel piles in the 3D model is about 0.4 m ($1.0B$), which is slightly higher than the height of the EPS in the 2D model, and about 0.1 m lower than that of the EPS in the 3D model.

4 Parametric study

The influence of fill height, pile clear spacing, friction coefficient, and porosity on the soil arching is summarized and presented in this section. The SCR and the maximum vertical displacement along the elevation at the maximum Δs were selected as two factors to investigate the load transfer mechanism and deformation characteristics.

4.1 Influence of fill height

The fill height directly influences the stress at the base of the embankment and governs the mode of soil arching (Lai et al., 2016; Rui et al., 2019). Fill heights ranging from 600 to 1400 mm, corresponding to h/B from 1.5 to 3.5, were used with a pile clear spacing of 400 mm. Fig. 15 indicates that increasing the fill height significantly increases the load transfer in both the 2D and 3D models. A lower value of SCR at the final stage than the maximum value indicates that the SCR increases initially and then decreases, irrespective of the chosen model. This also indicates that the load recovery effect exists in embankment with various fill heights, and a larger portion of fill weight is transferred onto subsoil with fill height increasing.

Fig. 16 presents the effect of the embankment height on the maximum vertical displacement. The results show that the settlement of soil along the elevation varies at different sections in the 3D embankment. When the embankment height is lower than 800 mm, soils in Part I sink deeper than surrounding fills and form a basin-like depression area (Fig. 14b). There is an ESP in the embankment, and the soil arch keeps a partial arching state. As a result, the increase of embankment height helps mainly to reduce the deformation in Part I, but has less influence on the soil

in Part II. The differential settlement at the crest reduces from 12.4 to 2.1 mm as the fill height increases from 600 to 800 mm. As the embankment height continues to increase, the soil arch enters into a fully mobilized arching state and keeps stable in terms of the settlement along the elevation. The surface settlement is almost 60% of the vertical displacement of the trapdoor. In the 2D model, settlement along the elevation at different embankment heights is almost the same, which is a trend similar to the behavior of soils at section s(b)-3D.

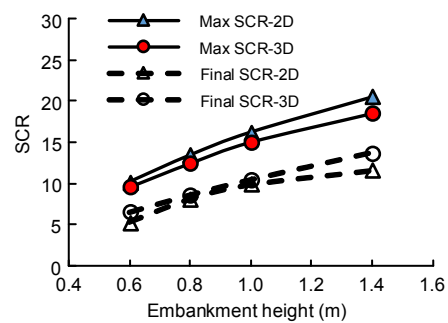


Fig. 15 Effect of embankment height on the SCR

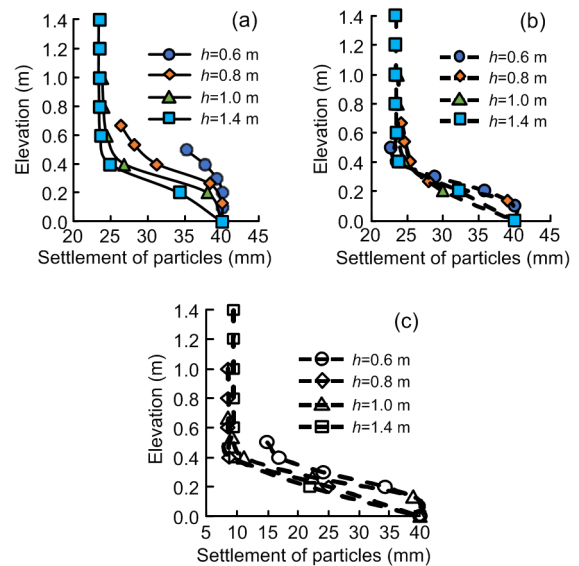


Fig. 16 Effect of embankment height h on the maximum vertical displacement at different sections

(a) Section s(a)-3D; (b) Section s(b)-3D; (c) Section s(b)-2D

4.2 Influence of pile clear spacing

The pile clear spacing B determines the area replacement ratio of the piles (e.g. a larger pile clear spacing implies a smaller area replacement ratio).

Figs. 17 and 18 show that a smaller pile clear spacing has a marked influence on increasing the load transfer and reducing the settlement (settlement at the crest and within the embankment) in both the 2D and 3D models, when the fill height is 1000 mm. The effects of the pile clear spacing on the SCR in both models are virtually the same at small pile clear spacing (e.g. $B=300$ mm), but vary as B increases. Increasing the pile clear spacing in 3D embankments can shorten the difference between the maximum SCR and the final SCR, and thus contributes to easing the influence of load recovery on the load transfer mechanism. The settlement reduction observed in the 2D model is not obvious in the 3D model. When the pile clear spacing is reduced from 500 to 300 mm, settlement at the crest in the 3D model is reduced 8 mm, which is nearly 2.7 times the settlement in the 2D model. In addition, the height of the ESP in 3D embankments increases with the increase in B . Lai et al. (2016) also indicated that the pile clear spacing would not change the arching feature and the maximum arching height is proportional to the pile clear spacing.

4.3 Influence of friction coefficient

The friction coefficient is one of the surface properties, which can resist the relative motion of particles. A high friction coefficient corresponds to large friction force. The friction angle is computed from triaxial test simulation. With the increase in the friction coefficient from 0.4 to 1.0, the friction angle changes from 25.8° to 31.4° . The effects of the friction coefficient on the SCR and settlement are presented in Figs. 19 and 20, where the embankment height is 1000 mm, which can form a fully mobilized soil arch. Increasing the friction coefficient can increase the degree of load transfer significantly and has a settlement reduction effect along the elevation in both the 2D and 3D models. But clearly, 2D models always have a higher peak SCR value and a lower final value than do 3D models. Therefore, more embankment load transfers back to the subsoil and an increase of the friction coefficient can contribute to this phenomenon. In addition, varying this parameter has no influence on the height of the ESP.

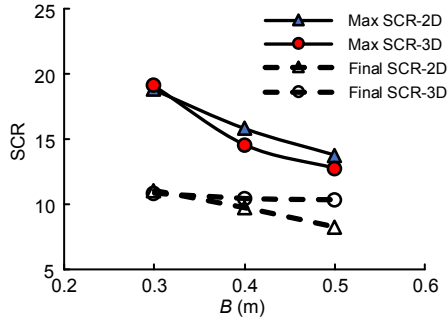


Fig. 17 Effect of the pile clear spacing B on the SCR

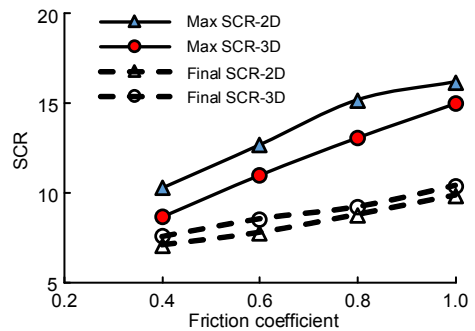


Fig. 19 Effect of the friction coefficient on the SCR

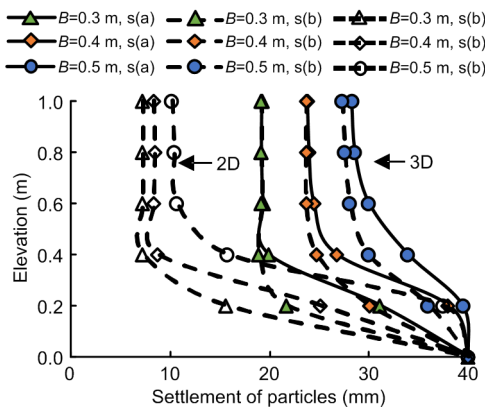


Fig. 18 Effect of the pile clear spacing B on the maximum vertical displacement

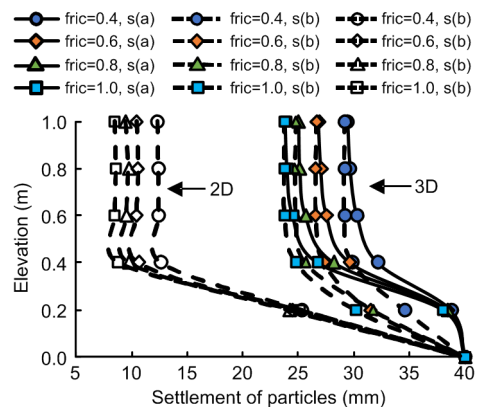


Fig. 20 Effect of the friction coefficient (fric) on the maximum vertical displacement

4.4 Influence of porosity

Embankment fills with different porosities have different densities, leading to different shear strength properties (Tran et al., 2019). A dense particle assembly tends to have a large shear strength during shearing, and a loose assembly has a small one. In this study, a porosity of 0.4 corresponded to a dense state, and 0.45 to a loose state. Fig. 21 demonstrates that different porosity values result in different evolutions of the SCR, when the embankment height is 1000 mm. When the porosity is larger than 0.42, the SCR increases continuously and then attains a constant value. During this process particles are gradually compacted from a loose state and the load transfer mechanism is enhanced accordingly. As the porosity decreases, the SCR increases first and then decreases, while the embankment fill tends to dilate from a dense state to a loose state and the load transfer mechanism weakens. In addition, a decrease of porosity from 0.45 to 0.40 leads to an increase of the SCR from 8.1 to 15.9 for 2D models, and from 7.2 to 14.9 for 3D models. Settlement reduction can be seen in Fig. 22, and has a more significant reduction effect than the other three factors (fill height, pile clear spacing, and

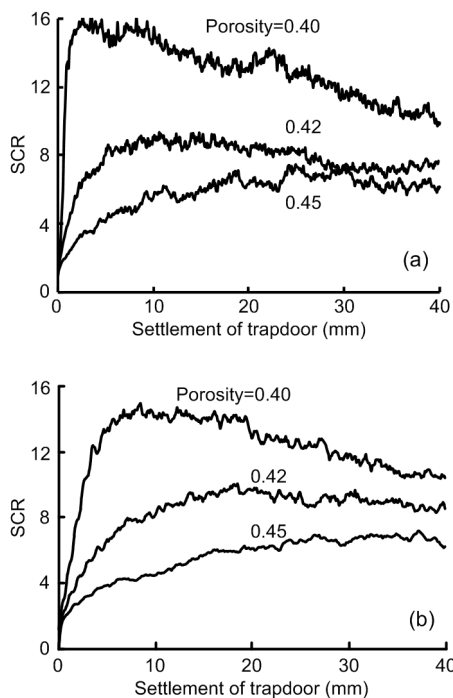


Fig. 21 Effect of the porosity on the SCR (a) 2D model; (b) 3D model

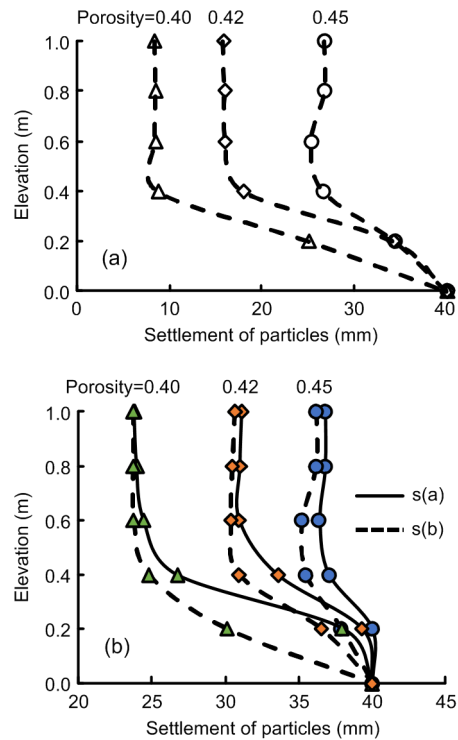


Fig. 22 Effect of the porosity on the maximum vertical displacement

(a) 2D model; (b) 3D model

friction angle). Moreover, settlement of soils at a loose state in the 2D embankment is closer to that in the 3D embankment at the same state.

5 Conclusions

To investigate the similarities and differences between a plane soil arch and a spatial soil arch in piled embankments, a series of 2D and 3D trapdoor numerical models were established using PFC3D. The results can be summarized as follows:

A plane soil arch reaches a larger degree of soil arching with less settlement of the trapdoor than a spatial soil arch at the maximum arching stage, and exerts a greater height of arching in terms of major principal stress. But due to a greater restriction through a larger soil interaction area in the 3D condition, the spatial arch forms a more stable arch foot in terms of stronger contacts above the pile cap at the loading recovery stage. The 2D embankment underestimated settlement at the crest and within the embankment because of moving only in one direction,

and had a lower ESP than the spatial arch which acts like a dome.

An increase of fill height and friction angle, and a decrease of pile clear spacing and porosity can help to improve the degree of load transfer and settlement reduction in both 2D and 3D embankments. Porosity has a more significant effect on reducing settlement than the other three factors. The height of the ESP increases as the pile clear spacing increases, but remains stable in 2D and 3D models whatever the embankment height, friction angle, and porosity. However, some differences emerge with respect to reducing the settlement of soils, especially for partially mobilized soil arching. Increasing fill height mainly reduces the settlement of soils in the portion of the 3D embankment above the square subsoil area, but has less influence on the portion above the rectangular subsoil area.

Acknowledgements

The authors appreciate the suggestions in English writing from Associate Professor Rajesh SATHIYAMOORTHY (Indian Institute of Technology, Kanpur, India).

Contributors

Ning BAO developed the DEM code and wrote the first draft of the manuscript. Wei JING and Jian-feng CHEN helped to organize the manuscript. Ping WEI revised and edited the final version.

Conflict of interest

Ning BAO, Jing WEI, Jian-feng CHEN, and Ping WEI declare that they have no conflict of interest.

References

Andrade JE, Chen QS, Le PH, et al., 2012. On the rheology of dilative granular media: bridging solid- and fluid-like behavior. *Journal of the Mechanics and Physics of Solids*, 60(6):1122-1136.
<https://doi.org/10.1016/j.jmps.2012.02.011>

Badakhshan E, Noorzad A, Bouazza A, et al., 2020. A 3D-DEM investigation of the mechanism of arching within geosynthetic-reinforced piled embankment. *International Journal of Solids and Structures*, 187:58-74.
<https://doi.org/10.1016/j.ijsolstr.2019.03.035>

Bhandari A, Han J, 2010. Investigation of geotextile-soil interaction under a cyclic vertical load using the discrete element method. *Geotextiles and Geomembranes*, 28(1): 33-43.
<https://doi.org/10.1016/j.geotexmem.2009.09.005>

Bhandari A, Han J, 2018. Two-dimensional physical modeling of soil displacements above trapdoors. *Geotechnical*

Research, 5(2):68-80.
<https://doi.org/10.1680/jgere.18.00002>

Briançon L, Simon B, 2012. Performance of pile-supported embankment over soft soil: full-scale experiment. *Journal of Geotechnical and Geoenvironmental Engineering*, 138(4):551-561.
[https://doi.org/10.1061/\(asce\)gt.1943-5606.0000561](https://doi.org/10.1061/(asce)gt.1943-5606.0000561)

BSI (British Standard Institution), 2010. Code of Practice for Strengthened/Reinforced Soils and Other Fills, BS8006-1. BSI, London, UK.

Cao WJ, Hu WW, 2014. Experimental study of 3D soil arching in piled reinforced embankments. *Rock and Soil Mechanics*, 35(2):351-358 (in Chinese).
<https://doi.org/10.16285/j.rsm.2014.02.027>

Chen YM, Cao WP, Chen RP, 2008. An experimental investigation of soil arching within basal reinforced and unreinforced piled embankments. *Geotextiles and Geomembranes*, 26(2):164-174.
<https://doi.org/10.1016/j.geotexmem.2007.05.004>

Chevalier B, Otani J, 2011. Arching observation in three-dimensional trapdoor problem with X-ray CT and discrete element method. *Soils and Foundations*, 51(3):459-469.
<https://doi.org/10.3208/sandf.51.459>

Costa YD, Zornberg JG, Bueno BS, et al., 2009. Failure mechanisms in sand over a deep active trapdoor. *Journal of Geotechnical and Geoenvironmental Engineering*, 135(11):1741-1753.
[https://doi.org/10.1061/\(asce\)gt.1943-5606.0000134](https://doi.org/10.1061/(asce)gt.1943-5606.0000134)

Das AK, Deb K, 2018. Experimental and 3D numerical study on time-dependent behavior of stone column-supported embankments. *International Journal of Geomechanics*, 18(4):04018011.
[https://doi.org/10.1061/\(asce\)gm.1943-5622.0001110](https://doi.org/10.1061/(asce)gm.1943-5622.0001110)

Dewoolkar MM, Santichaianant K, Ko HY, 2007. Centrifuge modeling of granular soil response over active circular trapdoors. *Soils and Foundations*, 47(5):931-945.
<https://doi.org/doi.10.3208/Sandf.47.931>

Eskişar T, Otani J, Hironaka J, 2012. Visualization of soil arching on reinforced embankment with rigid pile foundation using X-ray CT. *Geotextiles and Geomembranes*, 32:44-54.
<https://doi.org/10.1016/j.geotexmem.2011.12.002>

Han J, Gabr MA, 2002. Numerical analysis of geosynthetic-reinforced and pile-supported earth platforms over soft soil. *Journal of Geotechnical and Geoenvironmental Engineering*, 128(1):44-53.
[https://doi.org/10.1061/\(asce\)1090-0241\(2002\)128:1\(44\)](https://doi.org/10.1061/(asce)1090-0241(2002)128:1(44))

Han J, Bhandari A, Wang F, 2012. DEM analysis of stresses and deformations of geogrid-reinforced embankments over piles. *International Journal of Geomechanics*, 12(4): 340-350.
[https://doi.org/10.1061/\(asce\)gm.1943-5622.0000050](https://doi.org/10.1061/(asce)gm.1943-5622.0000050)

Han J, Wang F, Ai-Naddaf M, et al., 2017. Progressive development of two-dimensional soil arching with displacement. *International Journal of Geomechanics*,

- 17(12):04017112.
[https://doi.org/10.1061/\(asce\)gm.1943-5622.0001025](https://doi.org/10.1061/(asce)gm.1943-5622.0001025)
- Hewlett WJ, Randolph MF, 1988. Analysis of piled embankments. *Ground Engineering*, 21(3):12-18.
- Iglesia GR, Einstein HH, Whitman RV, 2011. Validation of centrifuge model scaling for soil systems via trapdoor tests. *Journal of Geotechnical and Geoenvironmental Engineering*, 137(11):1075-1089.
[https://doi.org/10.1061/\(asce\)gt.1943-5606.0000517](https://doi.org/10.1061/(asce)gt.1943-5606.0000517)
- Iglesia GR, Einstein HH, Whitman RV, 2014. Investigation of soil arching with centrifuge tests. *Journal of Geotechnical and Geoenvironmental Engineering*, 140(2):04013005.
[https://doi.org/10.1061/\(asce\)gt.1943-5606.0000998](https://doi.org/10.1061/(asce)gt.1943-5606.0000998)
- Jenck O, Dias D, Kastner R, 2007. Two-dimensional physical and numerical modeling of a pile-supported earth platform over soft soil. *Journal of Geotechnical and Geoenvironmental Engineering*, 133(3):295-305.
[https://doi.org/10.1061/\(asce\)1090-0241\(2007\)133:3\(295\)](https://doi.org/10.1061/(asce)1090-0241(2007)133:3(295))
- Jenck O, Dias D, Kastner R, 2009a. Discrete element modeling of a granular platform supported by piles in soft soil—validation on a small scale model test and comparison to a numerical analysis in a continuum. *Computers and Geotechnics*, 36(6):917-927.
<https://doi.org/10.1016/j.compgeo.2009.02.001>
- Jenck O, Dias D, Kastner R, 2009b. Three-dimensional numerical modeling of a piled embankment. *International Journal of Geomechanics*, 9(3):102-112.
[https://doi.org/10.1061/\(asce\)1532-3641\(2009\)9:3\(102\)](https://doi.org/10.1061/(asce)1532-3641(2009)9:3(102))
- Kempfert HG, Gobel C, Alexiew D, et al., 2004. German recommendations for reinforced embankments on pile-similar elements. Third European Conference on Geosynthetics, p.279-284.
- King DJ, Bouazza A, Gniel JR, et al., 2017. Load-transfer platform behaviour in embankments supported on semi-rigid columns: implications of the ground reaction curve. *Canadian Geotechnical Journal*, 54(8):1158-1175.
<https://doi.org/10.1139/cgj-2016-0406>
- Ladanyi B, Hoyaux B, 1969. A study of the trap-door problem in a granular mass. *Canadian Geotechnical Journal*, 6(1): 1-14.
<https://doi.org/10.1139/t69-001>
- Lai HJ, Zheng JJ, Zhang J, et al., 2014. DEM analysis of “soil”-arching within geogrid-reinforced and unreinforced pile-supported embankments. *Computers and Geotechnics*, 61:13-23.
<https://doi.org/10.1016/j.compgeo.2014.04.007>
- Lai HJ, Zheng JJ, Zhang RJ, et al., 2016. Visualization of the formation and features of soil arching within a piled embankment by discrete element method simulation. *Journal of Zhejiang University-SCIENCE A (Applied Physics & Engineering)*, 17(10):803-817.
<https://doi.org/10.1631/jzus.A1500302>
- Le Hello B, Villard P, 2009. Embankments reinforced by piles and geosynthetics—numerical and experimental studies dealing with the transfer of load on the soil embankment. *Engineering Geology*, 106(1-2):78-91.
<https://doi.org/10.1016/j.enggeo.2009.03.001>
- Marston A, 1930. The theory of external loads on closed conduits in the light of the latest experiments. The 9th Annual Meeting of the Highway Research Board, p.138-170.
- Rothenburg L, Bathurst RJ, 1993. Influence of particle eccentricity on micromechanical behavior of granular materials. *Mechanics of Materials*, 16(1-2):141-152.
[https://doi.org/10.1016/0167-6636\(93\)90037-R](https://doi.org/10.1016/0167-6636(93)90037-R)
- Rowe RK, Liu KW, 2015. Three-dimensional finite element modelling of a full-scale geosynthetic-reinforced, pile-supported embankment. *Canadian Geotechnical Journal*, 52(12):2041-2054.
<https://doi.org/10.1139/cgj-2014-0506>
- Rui R, van Tol AF, Xia XL, et al., 2016a. Evolution of soil arching; 2D DEM simulations. *Computers and Geotechnics*, 73:199-209.
<https://doi.org/10.1016/j.compgeo.2015.12.006>
- Rui R, van Tol AF, Xia YY, et al., 2016b. Investigation of soil-arching development in dense sand by 2D model tests. *Geotechnical Testing Journal*, 39(3):415-430.
<https://doi.org/10.1520/gtj20150130>
- Rui R, Han J, van Eekelen SJM, et al., 2019. Experimental investigation of soil-arching development in unreinforced and geosynthetic-reinforced pile-supported embankments. *Journal of Geotechnical and Geoenvironmental Engineering*, 145(1):04018103.
[https://doi.org/10.1061/\(asce\)gt.1943-5606.0002000](https://doi.org/10.1061/(asce)gt.1943-5606.0002000)
- Russell D, Naughton PJ, Kempton GT, 2003. A new design procedure for piled embankments. The 56th Canadian Geotechnical Conference and 2003 NAGS Conference, p.858-865.
- Song JH, Chen KF, Li P, et al., 2018. Soil arching in unsaturated soil with different water table. *Granular Matter*, 20(4):78.
<https://doi.org/10.1007/s10035-018-0849-3>
- Terzaghi K, 1943. *Theoretical Soil Mechanics*. John Wiley and Sons, New York, USA, p.66-76.
<https://doi.org/10.1002/9780470172766>
- Tien HJ, 1996. A Literature Study of the Arching Effect. MS Thesis, Massachusetts Institute of Technology, Cambridge, USA.
- Tran QA, Villard P, Dias D, 2019. Discrete and continuum numerical modeling of soil arching between piles. *International Journal of Geomechanics*, 19(2):04018195.
[https://doi.org/10.1061/\(asce\)gm.1943-5622.0001341](https://doi.org/10.1061/(asce)gm.1943-5622.0001341)
- van Eekelen SJM, Bezuijen A, Lodder HJ, et al., 2012a. Model experiments on piled embankments. Part I. *Geotextiles and Geomembranes*, 32:69-81.
<https://doi.org/10.1016/j.geotextmem.2011.11.002>
- van Eekelen SJM, Bezuijen A, Lodder HJ, et al., 2012b. Model experiments on piled embankments. Part II. *Geotextiles and Geomembranes*, 32:82-94.
<https://doi.org/10.1016/j.geotextmem.2011.11.003>
- van Eekelen SJM, Venmans AAM, Bezuijen A, et al., 2020. Long term measurements in the Woerden geosynthetic-

reinforced pile-supported embankment. *Geosynthetics International*, 27(2):142-156.

<https://doi.org/10.1680/jgein.17.00022>

Xu C, Zhang XY, Han J, et al., 2019. Two-dimensional soil-arching behavior under static and cyclic loading. *International Journal of Geomechanics*, 19(8):04019091.

[https://doi.org/10.1061/\(asce\)gm.1943-5622.0001482](https://doi.org/10.1061/(asce)gm.1943-5622.0001482)

Zhu B, Gao D, Li JC, et al., 2012. Model tests on interaction between soil and geosynthetics subjected to localized subsidence in landfills. *Journal of Zhejiang University-SCIENCE A (Applied Physics & Engineering)*, 13(6): 433-444.

<https://doi.org/10.1631/jzus.A1100315>

Zhuang Y, Wang KY, 2015. Three-dimensional behavior of biaxial geogrid in a piled embankment: numerical investigation. *Canadian Geotechnical Journal*, 52(10):1629-1635.

<https://doi.org/10.1139/cgj-2014-0538>

中文概要

题目: 桩承式路堤二维和三维土拱效应离散元分析

目的: 土拱效应是桩承式路堤的主要荷载传递机理。本文旨在探讨随着桩土差异沉降量的增加, 平面土拱和空间土拱演化过程中的相似点和差异性, 以深化对桩承式路堤作用机制的理解。

创新点: 1. 基于离散元法对比分析平面土拱和空间土拱的

作用发挥机制, 包括细观角度的强弱力链分布特征和宏观角度的沉降变形模式; 2. 探讨路堤设计参数和土体参数对二维和三维路堤荷载传递和沉降变形(路堤顶面和路堤内部)的影响。

方法: 1. 基于活动门室内模型试验建立桩承式路堤二维和三维离散元数值模型; 依据接触力均值划分强弱力链, 得到土拱结构的分布特征; 采用颗粒位移分组获取土体变形模式。2. 通过变化路堤高度、桩净间距、填料内摩擦角以及孔隙率来分析路堤荷载和变形响应。

结论: 1. 平面土拱效应存在高估路堤荷载传递效率和低估路堤沉降变形的现象。2. 当路堤高度高于等沉面, 即土拱结构处于全拱状态时, 路堤土体的空间滑裂面表现为穹顶状, 且等沉面位置高于二维模型。3. 增大路堤高度和填料内摩擦角以及减小桩净间距和孔隙率都能够提高平面土拱和空间土拱的荷载传递能力, 进而减小路堤沉降量; 其中, 孔隙率对沉降变形的影响最为明显。4. 当路堤高度低于等沉面, 即土拱结构处于非全拱状态时, 在三维模型中增加路堤高度主要减小四桩间上部土体沉降, 而对两桩间上部土体沉降的影响较小。

关键词: 桩承式路堤; 土拱效应; 离散元法; 荷载传递; 沉降变形